Constraining the Impact of Dust-Driven Droplet Freezing on Climate Using Cloud-Top-Phase Observations

AGU ADVANCING EARTH AND SPACE SCIENCE

Geophysical Research Letters

RESEARCH LETTER
10.1029/2021GL092687

Constraining the Impact of Dust-Driven Droplet Freezing on Climate Using Cloud-Top-Phase Observations

Diego Villanueva[1], David Neubauer[2], Blaž Gasparini[3,4], Luisa Ickes[5], and Ina Tegen[1]

[1]Modelling Department, Institute for Tropospheric Research (TROPOS), Leipzig, Germany, [2]Institute for Atmospheric and Climate Science, ETH Zürich, Zürich, Switzerland, [3]Department of Atmospheric Sciences, University of Washington, Seattle, WA, USA, [4]Now at Department of Meteorology and Geophysics, University of Vienna, Vienna, Austria, [5]Department of Space, Earth and Environment, Chalmers University, Gothenburg, Sweden

Abstract Despite advances in our understanding of ice-nucleating particles, the effect of cloud glaciation on the Earth's radiation balance has remained poorly constrained. Particularly, dust ice nuclei are believed to enhance cloud glaciation in the Northern Hemisphere. We used satellite observations of the hemispheric and seasonal contrast in cloud top phase to assess the dust-driven droplet freezing in a climate model. The required freezing efficiency for dust ice nuclei suggests that climate models glaciate too few clouds through immersion droplet freezing. After tuning, the model leads to more realistic cloud-top-phase contrasts and a dust-driven glaciation effect of 0.14 ± 0.13 W m^{-2} between 30°N and 60°N. Observations of cloud-top-phase contrasts provide a strong constraint for ice formation in mixed-phase clouds and may provide a weak constraint for the associated impact on radiation and precipitation. Future studies should therefore consider both the mean-state cloud-phase partitioning and cloud-phase contrasts to achieve a more accurate simulation of dust-driven cloud glaciation.

Plain Language Summary Between 0°C and −38°C, clouds can be composed of cloud droplets (water), ice crystals, or some combination of the two. Water clouds reflect much more sunshine back to space compared to ice clouds and therefore have a larger cooling effect on climate. Some atmospheric particles like dust can transform water clouds into ice clouds. The Northern Hemisphere contains more of such particles, which leads to more ice clouds, as confirmed by satellite observations. We such satellite observations to constrain the effect of cloud freezing in climate models and its impact on climate. This helps make climate models and their projections of future climate more realistic.

Key Points:

- Two droplet freezing schemes were assessed using satellite observations of the hemispheric and seasonal contrast in cloud top phase
- Our results suggest a previous underestimation of dust-driven droplet freezing, especially for high dust concentrations
- At midlatitudes, the dust-driven glaciation with the tuned scheme results in a radiative effect of 0.14 ± 0.13 W m^{-2}

Supporting Information:

Supporting Information may be found in the online version of this article.

Correspondence to:

D. Villanueva,
villanueva@tropos.de

Citation:

Villanueva, D., Neubauer, D., Gasparini, B., Ickes, L., & Tegen, I. (2021). Constraining the impact of dust-driven droplet freezing on climate using cloud-top-phase observations. *Geophysical Research Letters*, *48*, e2021GL092687. https://doi.org/10.1029/2021GL092687

Received 27 JAN 2021
Accepted 22 MAY 2021

Author Contributions:

Conceptualization: Diego Villanueva, David Neubauer, Blaž Gasparini, Luisa Ickes, Ina Tegen
Formal analysis: Diego Villanueva
Investigation: Diego Villanueva
Visualization: Diego Villanueva
Writing – original draft: Diego Villanueva
Writing – review & editing: David Neubauer, Blaž Gasparini, Luisa Ickes, Ina Tegen

1. Introduction

Aerosol–cloud interactions, especially for ice and mixed-phase clouds, are a major source of uncertainty for predicting weather and climate change (Bellouin et al., 2020; Forbes & Ahlgrimm, 2014; McCoy et al., 2016). On average, clouds cool the planet; however, the cloud radiative effect (CRE) depends strongly on the number and size of hydrometeors (Seinfeld et al., 2016). Particularly, cloud optical thickness is tied to the hydrometeor surface area. Thus, a cloud with a large number of small hydrometeors will be more reflective compared to a cloud of the same condensed water content composed of a small number of large hydrometeors (Twomey, 1974). Moreover, a cloud composed of larger hydrometeors will be shorter lived: the larger hydrometeors will precipitate faster out of the atmosphere (Albrecht, 1989).

Ice-nucleating particles (INPs) can trigger droplet freezing between 0°C and −35°C (Hoose & Möhler, 2012); subsequently, ice particles grow at the expense of depleting liquid cloud droplets (Bergeron, 1935; Findeisen et al., 2015; Wegener, 1911). The number of ice particles is typically orders of magnitude smaller compared to the number of cloud droplets and their size is several times larger than the typical cloud droplet size. Therefore, at temperatures warmer than −35°C, INP-driven droplet freezing is associated with less reflecting clouds and a warming effect on climate (IPCC et al., 2007; Lohmann & Diehl, 2006; Shi & Liu, 2019; Yun & Penner, 2013; Yun et al., 2013).

In climate models, droplet freezing schemes are based on field measurements (e.g., DeMott et al., 2010), laboratory measurements (e.g., Lohmann & Diehl, 2006; Niemand et al., 2012), or theoretical frameworks, as Classical Nucleation Theory (Hoose et al., 2010; Ickes et al., 2017). In this study, we compare two

laboratory-based freezing schemes for immersion freezing that have been already tested with the ECHAM-HAM climate model (Hoose et al., 2008; Huang et al., 2018; Ickes, 2015).

Although many natural and anthropogenic aerosols are known to act as INP, most evidence suggests that cloud glaciation at temperatures colder than −15°C is dominated by mineral dust (Kawamoto et al., 2020; Tan et al., 2014; Vergara-Temprado et al., 2017; Villanueva et al., 2020; Zhang et al., 2018). Ice cloud frequency and mineral dust concentrations observed from space are higher in the Northern Hemisphere, as well as during boreal and austral spring (Bruno et al., 2021; Cowie et al., 2014; Hu et al., 2010; Tan et al., 2014; Villanueva et al., 2021; Wu et al., 2020; Zhang et al., 2018). In addition, dust emissions may have increased by about 25% since preindustrial times due to land use change (Stanelle et al., 2014). Therefore, to better understand the impacts of current atmospheric dust and of climate change, it is essential to better constrain the radiative effect of dust-driven cloud glaciation (Shi & Liu, 2019).

Previous studies have relied on atmospheric state observations of dust loading (Shi & Liu, 2019) and ice cloud frequency (Tan et al., 2016) to assess cloud glaciation. However, observational constraints for process rates can lead to a better estimation of aerosol–cloud interactions (Mülmenstädt et al., 2020). Furthermore, a better understanding of cloud glaciation may help to better represent the cloud-phase feedback and climate sensitivity in climate models (Murray et al., 2021). Therefore, in this study, we use the hemispheric and seasonal contrast of cloud top phase based on satellite observations to improve dust-driven immersion freezing and its impact on climate in ECHAM-HAM.

2. Methods

2.1. Model Description

For our study, we use a state-of-the-art atmospheric model able to represent aerosol–cloud interactions with sufficient detail. The aerosol–climate model ECHAM(v6.3.0)-HAM(v2.3) (Neubauer et al., 2019; Tegen et al., 2019) is coupled to the Predicted bulk Particle Properties (P3) microphysical scheme newly implemented in ECHAM-HAM (Dietlicher et al., 2018, 2019; Morrison & Milbrandt, 2015) with the "2M" tuning configuration (Dietlicher et al., 2018). The nudged simulations were performed for the period 2003–2012 using 31 vertical model layers, a horizontal resolution of 1.875°(T63), and interactively computed dust emissions (Tegen et al., 2019, see Text S2).

2.2. Satellite Simulator and A-Train Observations

To enable a direct comparison between model and observations, we use a satellite simulator and two different satellite phase products. The CFMIP Observation Simulator Package (COSP v2.0; Swales et al., 2018) was used in the model to recreate the satellite retrievals of cloud phase. Specifically, we used the lidar simulator, which provides 3D cloud-phase classification. For the COSP outputs, we use the cloud phase in the highest cloudy gridbox and the temperature at the top of the highest cloudy gridbox. The GCM-Oriented CALIPSO Cloud Product (CALIPSO-GOCCP; Cesana & Chepfer, 2013; Chepfer et al., 2010) is a cloud-phase product based on spaceborne lidar retrievals and is the counterpart to the COSP simulator. In the satellite product, we define the cloud top as the highest cloudy pixel of the retrieval. To account for potential biases in the GOCCP product and provide a margin of error for the observations, we also included the GDP (GOCCP-DARDAR-PML2) product ensemble (Villanueva et al., 2021). In the observations, the narrow swaths of the satellites are averaged over 2° × 30°(lat × lon) boxes for a whole month to ensure that the sample size is high enough for a robust frequency estimate. After averaging the observations zonally, the 2°latitude bands fit well with the model resolution of 1.875°. We did not filter out convective clouds. However, the cloud top phase is dominated by stratiform clouds (Villanueva et al., 2021).

2.3. Freezing Schemes

The heterogeneous freezing scheme in the reference version of ECHAM-HAM is the Lohmann–Diehl (LD) scheme (Hoose et al., 2008; Lohmann & Diehl, 2006), which is based on wind tunnel experiments. In this parameterization, the immersion freezing rate J_{imm} depends on the dust particle number concentration in the soluble mode $N_{imm,dust}$, temperature (T [°C]), turbulent kinetic energy (TKE), and on the number

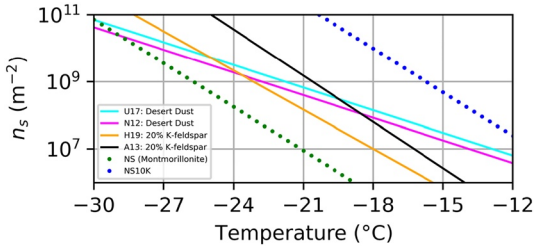

Figure 1. Ice active surface site density of natural dust n_s for the simulations **NS** (montmorillonite), **NS10K**, and for different state-of-the-art parameterizations for dust-INP: U17 (Ullrich et al., 2017), N12 (Niemand et al., 2012), H19 (Harrison et al., 2019), and A13 (Atkinson et al., 2013). INP, ice-nucleating particle.

concentration of ambient cloud condensation nuclei (CCN; Lohmann et al., 2007). The immersion freezing rate is calculated as

$$J_{imm} = N_a \cdot c_{dust} \frac{N_{imm,dust}}{CCN} e^{-N_a \cdot (T)} \frac{dT}{dt} \frac{\rho_{air} \cdot q_l}{\rho_l} (\mathrm{m^{-3}s^{-1}}), \quad (1)$$

$$\frac{dT}{dt} = \frac{\omega_{largescale} - 0.7\sqrt{TKE} \cdot \rho_{air} \cdot g}{c_p \cdot \rho_{air}}, \quad (2)$$

with $\omega_{largescale}$ the large-scale term from the vertical velocity, q_l the cloud liquid water mass-mixing ratio, ρ_{air} the air density, ρ_l the cloud droplet density, g the gravitational constant, c_p the specific heat of air, and $N_a = 1°\mathrm{C}^{-1}$. The freezing efficiency ($c_{dust} = 32.3$) is assumed to have the freezing efficiency of montmorillonite in the reference configuration (Claquin et al., 1999; Hoose et al., 2008).

The second freezing scheme used in this study is based on cloud chamber experiments (NS; e.g., Connolly et al., 2009; Huang et al., 2018; Ickes et al., 2017; Niemand et al., 2012). In this parameterization, the fraction of frozen droplets *FF* increases linearly with the dust particle surface area A_j and the ice active surface site density of natural dust n_s, which depends on the aerosol characteristics N_A and N_B, with

$$FF = 1 - e^{-A_j \cdot n_s(T)}, \quad (3)$$

$$n_s(T) = e^{-N_A \cdot (T - N_B)} (\mathrm{m^{-2}}). \quad (4)$$

Similar to the LD scheme, we set the temperature dependence ($N_A = 1°\mathrm{C}^{-1}$) and temperature offset ($N_B = -5°\mathrm{C}$) similarly to what observed for montmorillonite (Ickes et al., 2017). In addition, to assess the sensitivity of the freezing scheme to different INP efficiencies, we increased the temperature offset N_B for which dust can trigger immersion freezing by +10°C for simulations **NS10K** and **NS-Tuned**. Figure 1 shows the ice active surface site density for montmorillonite (**NS**) and **NS10K** relative to different surrogates for dust-INP in the literature. The temperature shift from **NS** to **NS10K** is equivalent to increasing INP concentrations by about 4 orders of magnitude (see Equation 4).

Although both the LD and NS schemes represent the same process of immersion freezing, the LD scheme predicts a freezing rate while the NS scheme predicts a fraction of frozen droplets. The NS scheme is deterministic and time independent, so that droplet freezing stops after the predicted number of frozen droplets is reached (Ickes, 2015). In contrast, in the LD scheme, the freezing rate is a time-dependent prognostic quantity and does not consider the number of already frozen droplets (Hoose et al., 2008).

In general, climate models do not keep track of INPs directly. Therefore, INPs that have been already activated are not removed for future iterations. Consequently, it may be useful to introduce a threshold to limit droplet freezing in clean conditions. In such conditions, the few INPs that may have been present are probably already depleted or deactivated by aging processes such as sulfate coating (Cziczo et al., 2009).

2.4. Model Simulations

We can separate the simulations in this study in three major groups, each addressing a different aspect of the immersion freezing parameterization: scheme type (group I: **LD** and **NS**), INP efficiency (group II: **NS** and **NS10K**), and dust threshold (group III: **NS10K** and **NS-Tuned**). A diagram showing this structure, together with the tuning strategy behind it, can be found in Figure S1. Additional simulations for group II and group III with different parameter values can be found in the supporting information (Table S1 and Figures S3–S5).

For all simulations, contact freezing and deposition nucleation in the mixed-phase regime are turned off. In the **NoFRZ** simulation, immersion freezing is turned off, but droplets are converted to ice at −35°C (homogenous freezing). The **LD** and **NS** simulations use the LD and NS scheme, respectively, and assume the

INP efficiency of the clay mineral montmorillonite. In the **NS10K** simulation, shifting N_B by +10°C causes dust-INP to freeze at temperatures 10°C warmer compared to the **NS** simulation. The **NS-Tuned** simulation is based on the **NS10K** simulation, but only dust number concentrations higher than 10^6 kg^{-1} are considered for droplet freezing. This threshold compensates the overestimation of dust-driven cloud glaciation in the Southern Hemisphere, which we believe to be related to the lack of INP tracking in the model. Thus, compared to the default configuration in **LD**, in **NS-Tuned** we use a different freezing scheme, a higher dust-INP efficiency, and a threshold for dust-INP concentrations.

2.5. Quantifying Cloud Glaciation and Cloud-Top-Phase Contrasts

The cloud top is usually the coldest part of the cloud and thus more sensitive to heterogeneous freezing. In addition, many satellite instruments are only sensitive to cloud top properties. To isolate the impact of each freezing parameterization on cloud top phase, we compare each simulation with a reference scenario, where droplets only freeze at temperatures colder than −35°C. We define the fraction of *dust-driven* glaciated cloud tops ("glaciated fraction") as the difference between the cloud top ice frequency (CIF) for each simulation and the **NoFRZ** simulation, normalized by the frequency of liquid clouds in **NoFRZ** at each temperature bin of 3°C.

$$\text{Glaciated fraction} = \frac{CIF_{simulation} - CIF_{NoFRZ}}{1 - CIF_{NoFRZ}}. \tag{5}$$

We focus on the midlatitudes, since here the hemispheric and seasonal variability of cloud-phase is higher (Villanueva et al., 2021; Zhang et al., 2018), and the radiative effect of dust-INP is stronger compared to the high latitudes and subtropics (between −35°C and 0°C; Lohmann & Diehl, 2006; Shi & Liu, 2019).

To quantify and evaluate the hemispheric and seasonal contrast in cloud top phase against observations, we normalize the contrast in CIF (spring–fall or north–south) by the liquid cloud frequency in the "clean" part of the contrast (i.e., where dust loading is low, as during fall or in the Southern Hemisphere). To avoid artifacts from low sample sizes, we only use the observed cloud-top-phase contrast for temperatures where the liquid cloud frequency is higher than 10%.

$$\text{Cloud - phase contrast} = \frac{CIF_{dusty} - CIF_{clean}}{1 - CIF_{clean}} \tag{6}$$

$$dusty - clean = \begin{cases} north - south, & \text{hemispheric} \\ spring - fall, & \text{seasonal} \end{cases} \tag{7}$$

We assess the agreement between simulated and observed cloud-phase contrast by the average difference between −35°C and 0°C.

3. Results

3.1. Dust-Driven Cloud Glaciation

The dust loading at each hemisphere and the choice of freezing scheme affects how many clouds glaciate, especially for temperatures colder than −15°C. Figures 2a and 2b show the fraction of cloud liquid tops that glaciate due to dust-INP for each simulation in the midlatitudes. For temperatures colder than −35°C, all droplets are forced to freeze in the model, causing the dust-driven glaciated fraction to drop (not shown). For temperatures warmer than −15°C, the INP efficiency is often too low for dust aerosol to glaciate liquid clouds, and the glaciated fraction drops to zero as well. Between 30°N and 60°N, the fraction of dust-driven glaciated cloud tops is almost identical for the **LD** and **NS** simulations, increasing from −25°C until −35°C (Figure 2a).

In terms of temperature difference, a shift in dust-INP efficiency is translated to an even stronger shift in dust-driven cloud glaciation (Figure 2a). For the **NS** simulation, at 30°N–60°N, the highest fraction of cloud tops glaciate at −34°C, where about 40% glaciate. For **NS10K**, the temperature where as many (40%)

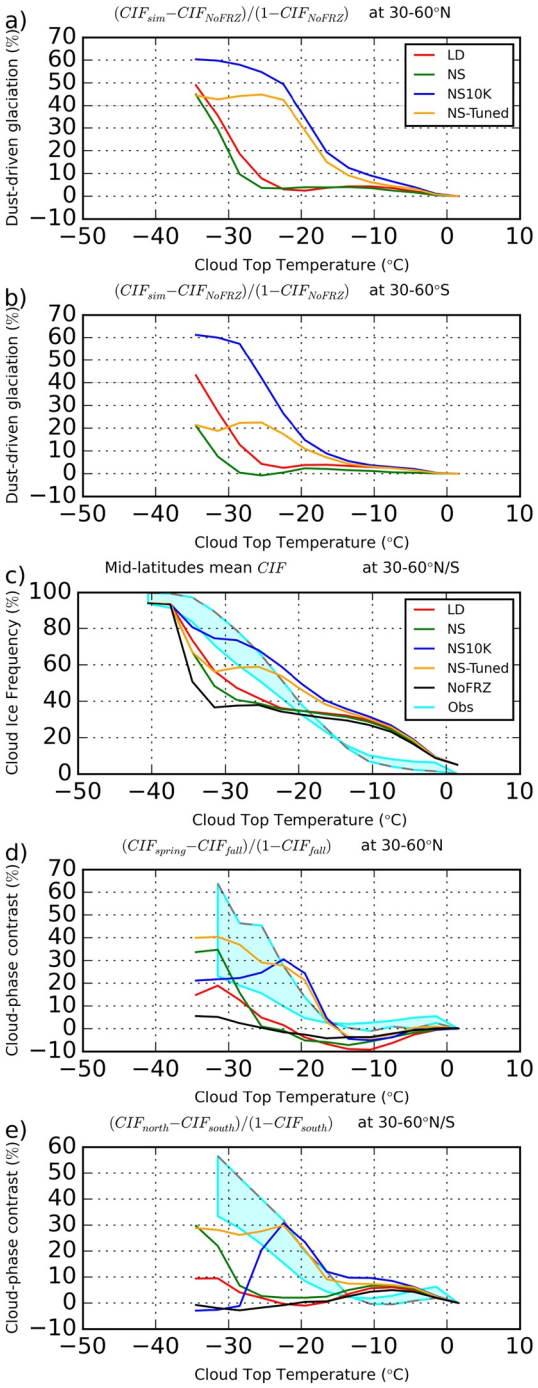

Figure 2. (a, b) Fraction of the liquid clouds (in the NoFRZ simulation) that glaciate in each simulation at (a) 30°N–60°N and (b) 30°S–60°S. (c) Cloud top ice frequency (CIF) at the midlatitudes. (d) Fraction of clouds additionally glaciated at 30–60°N during spring (compared to fall) normalized by the fraction of liquid clouds during fall. (e) Fraction of clouds additionally glaciated at 30°N–60°N (compared to 30°S–60°S) normalized by the fraction of liquid clouds at 30°S–60°S. The limit of the observations corresponds to the GOCCP product and GDP ensemble (dashed), respectively (2007–2010). The light blue shading highlights the difference between the two observational products. Each datapoint corresponds to a 3°C temperature bin.

liquid cloud tops glaciate is $T_{40\%} = -21$°C, about +13°C warmer than for **NS**. Recalling Section 2.4, in the **NS10K** simulation dust leads to droplet freezing at warmer temperatures (+10°C) compared to **NS**. However, dust concentrations—and therefore droplet freezing—increase at warmer temperatures, enhancing the difference in the dust-driven cloud glaciation temperature $T_{40\%}$ between **NS** and **NS10K**.

In ECHAM-HAM, the increase in dust-driven glaciation for lower temperatures is weaker after setting a threshold for dust concentration, such that only high dust concentrations can lead to droplet freezing. At −35°C, in simulation **NS10K** the glaciated fraction converges to about 60% in both hemispheres (Figures 2a and 2b). Using 10^6 kg^{-1} as a threshold of dust particle concentration for initiating freezing, starting at −25°C the glaciated fraction in **NS-Tuned** decreases compared to **NS10K** and remains rather constant for lower temperatures. Specifically, the glaciated fraction caps at 43% and 21% for the northern and southern midlatitudes, respectively. The impact of the threshold in **NS-Tuned** is higher at lower temperatures and in the Southern Hemisphere, where dust concentrations tend to be lower.

For all simulations, fewer cloud tops glaciate at 30°S–60°S compared to 30°N–60°N (Figure 2b). However, for **LD** this hemispheric difference in cloud glaciation is weaker compared to the simulations using the NS scheme. This hemispheric contrast in **NS** is a result of the higher aerosol dust loading in the Northern Hemisphere, which is the only variable controlling the droplet freezing rate in the NS scheme besides temperature. In contrast, the LD scheme is less sensitive to contrasts in dust loading (discussed in Section 4.2).

3.2. Satellite Constraints to Cloud Glaciation

In ECHAM-HAM, the mean-state cloud ice frequency is dominated by ice formation at temperatures colder than −35°C, while the seasonal and hemispheric contrasts in cloud top phase are dominated by dust-driven droplet freezing between −35°C and −15°C. Figures 2c–2e show the simulated frequency of ice cloud tops *CIF* and the hemispheric and seasonal contrast in cloud top phase together with observations. Both the modeled and observed *CIF* increase from 0%–10% to 90%–100% between 0°C and − 35°C (Figure 2c). Between − 35°C and − 15°C, *CIF* is higher for the GDP than for the GOCCP observations. In the same temperature range, *CIF* varies on average by up to 30% between the **NoFRZ**, **NS**, **LD**, **NS-Tuned**, and **NS10K** simulations (ordered from lower to higher *CIF*). Between −35°C and 0°C, most of the ice clouds from the different simulations persist in the **NoFRZ** simulation. This implies that most of such ice clouds, especially for temperatures between −35°C and −15°C, have their origin at lower temperatures where cloud droplets can freeze without INP (Dietlicher et al., 2019). For our tuning strategy, this means that the droplet freezing parameterization alone cannot explain the disagreement in the frequency of ice cloud tops between model and observations (discussed in Section 4.4c; see also a comparison with the E3SM model in Figure S2a). However, the seasonal and the hemispheric contrasts are controlled by dust-driven droplet freezing. Indeed, in the model both contrasts are negligible without heterogeneous freezing (Figures 2d and 2e; discussed in Section 4.1).

The contrast in cloud top phase improves compared to observations after tuning the model by choosing the NS scheme over the LD scheme, by increasing the dust-INP efficiency, and by including a dust threshold. The observed seasonal (Figure 2d) and hemispheric (Figure 2e) contrasts of cloud top phase increase between −15°C and −30°C from 0%–5% up to 20%–30% for the GOCCP and up to 50%–60% for the GDP observations. In this temperature range, the contrasts increase with decreasing temperatures for the **NS**, **LD**, and **NS-Tuned** simulations (ordered from lower to higher contrast). For temperatures colder than −15°C, **NS** results in a better agreement with the observed phase contrasts compared to **LD**, especially against the GDP observations. Furthermore, the hemispheric and seasonal contrasts are higher for the **NS-Tuned** simulation than for **NS** at all temperatures, leading to a better agreement with observations. First, the higher INP efficiency in **NS10K** shifts the temperature range of the cloud-top-phase contrast to warmer temperatures. The **NS10K** simulation was selected from a wider range of simulations (N_B steps of 2.5°C) because it produces the best agreement with the observed cloud-top-phase contrasts between −15°C and −30°C (see supporting information S3 and S5). We choose this range because for temperatures warmer than −15°C, INP efficiency is too low to trigger glaciation; while for temperatures colder than −30°C, liquid clouds are too rare to derive a robust contrast in cloud phase. Second, the implementation of a dust threshold in **NS-Tuned** increases the magnitude of the cloud-top-phase contrast by inhibiting droplet freezing in clean environments. We tested several thresholds, from which 10^6 kg^{-1} resulted in the best agreement with the observed cloud-top-phase contrasts, especially between −15°C and −30°C (see Figure S4). As a result, **NS-Tuned** agrees better with the high-contrast (GDP) reference compared to **NS** for both the seasonal and hemispheric contrasts.

3.3. Other Climate Models

Using another state-of-the-art climate model, we found that the NS scheme with enhanced dust-INP efficiency improves the cloud-phase contrast in a similar way as observed in ECHAM-HAM. To validate our approach, we run several simulations including **NS** and **NS10K** with the E3SM aerosol–climate model (Rasch et al., 2019) for 1 year. In the E3SM model, the best agreement with the observed contrasts was found for the **NS10K** simulation (see Figure S2).

3.4. Climate Implications

Besides the changes in the ice cloud frequency, the dust-driven droplet freezing parameterization impacts key microphysical parameters related to radiation and precipitation. Table 1 summarizes these changes due to dust-INP, compared to **NoFRZ**. Although the magnitude of these changes varies, the sign of the changes is the same for both hemispheres and for all freezing parameterizations.

Dust-driven droplet freezing increases the ice water path (IWP) and reduces the cloud Liquid Water Path (LWP) depending mainly on the freezing scheme used. At 30°N–60°N, the increase in IWP relative to **NoFRZ** (ΔIWP) is about twice as high for **NS-Tuned** compared to **LD**, which is consistent with the increase in cloud glaciation discussed in Section 3.1. Although dust-driven cloud glaciation and ΔIWP are higher for **NS-Tuned** than for **LD**, ΔLWP is lower in magnitude for **NS-Tuned** compared to **LD**, which is a rather counterintuitive result (discussed in Section 4.2). For **LD**, ΔLWP and ΔIWP are symmetric between hemispheres (the differences are below ±20% between 30°N–60°N and 30°S–60°S). In contrast, for **NS-Tuned** ΔLWP and ΔIWP are about twice as high at 30°N–60°N compared to 30°S–60°S.

The change in cloud cover (CC) due to dust-INP is similar for the **LD** and **NS-Tuned** simulations but highly asymmetric between hemispheres: −1.3% on average at 30°N–60°N and −0.2% at 30°S–60°S. However, ΔCC is too small to explain the large changes in shortwave (SW) CRE and longwave (LW) CRE. For **LD**, the increase in SW CRE due to dust-INP is about twice in magnitude compared to the decrease in LW CRE, suggesting a reduction of more reflective clouds (SW CRE > LW CRE), which explains the higher net ΔCRE in **LD** compared to **NS-Tuned**. In contrast, for **NS-Tuned**, both ΔSW CRE and ΔLW CRE are similar in magnitude (within ±15%), suggesting a reduction of less reflective clouds (SW CRE ∼ LW CRE).

Dust-driven droplet freezing leads to a weak increase in Net CRE at the midlatitudes. The Net ΔCRE for **LD** and **NS-Tuned** appears to be associated with ΔLWP (discussed in Section 4.2). However, for **NS-Tuned**

Table 1
Changes in Key Microphysical Parameters due to Dust-INP at the Mid-latitudes

Simulations latitude: 30°–60°	NoFRZ (°N)	ΔLD (°N)	σ_{LD} (°N)	ΔLD (°S)	ΔNS-Tuned (°N)	σNS-Tuned (°N)	ΔNS-Tuned (°S)
IWP, g m^{-2}	63.44	3.08	0.16	3.34	6.26	0.33	2.95
LWP, g m^{-2}	158.40	**−30.65**	0.76	**−25.20**	−19.79	0.96	−9.81
Net CRE, W m^{-2}	−34.12	1.48	0.16	1.55	*0.14*	0.13	*0.12*
CC, %	69.60	−1.22	0.15	*−0.25*	−1.43	0.22	*−0.23*
SW CRE, W m^{-2}	−56.17	3.23	0.18	2.92	2.12	0.19	1.11
LW CRE, W m^{-2}	22.04	−1.74	0.09	−1.37	−1.98	0.13	−0.98
P_{strat}, 10^{-1} mm day^{-1}	1.57	0.12	0.03	0.12	0.24	0.02	0.13
P_{cnv}, 10^{-1} mm day^{-1}	0.77	*−0.01*	0.02	−0.04	−0.10	0.02	*−0.01*
N_i, 10^8 m^{-2}	11.36	−0.52	0.13	−0.33	*−0.04*	0.30	*−0.17*
N_c, 10^{10} m^{-2}	8.69	−1.60	0.05	−0.63	−1.10	0.09	−0.34

Note. Calculated as the difference of the LD and NS-Tuned simulations compared to the NoFRZ simulation. The table also highlights for which variables the change due to dust-INP is not significant (within ±2σ; in italics), remarkably asymmetric (at least 150% at 30°N–60°N relative to 30°S–60°S; underlined), and particularly high (at least ±10% relative to the average at 30°N–60°N; in bold). The error σ corresponds to the interannual (2003–2012) standard deviation of the annual-field averages at 30°N–60°N.

ΔCRE is closer to a previous estimation (0.34 W m^{-2} between 30°N and 70°N; Shi & Liu, 2019). In agreement with Shi and Liu (2019), we find a cooling effect (of at least −0.5 W m^{-2}) for all simulations northern from 70°N related to a decrease in CC and LW CRE, because clouds there have on average a warming effect (SW CRE < LW CRE; see Figures S8 and S11). Due to the water depletion by dust-INP, the overall radiative effect of clouds gets weaker. Thus, a weaker cloud warming effect near the poles results in an overall cooling effect. In contrast to Shi and Liu (2019), we found the dust-driven glaciation effect ΔCRE to be symmetric (within ±20%) within hemispheres.

Due to dust-INP, stratiform precipitation P_{strat} is enhanced at the expense of convective precipitation P_{conv}. For **LD**, P_{strat} increases by about +0.012 mm day^{-1} (+8%, see also Figure S12). At 30°N–60°N, in **NS-Tuned** P_{strat} is enhanced by +0.024 mm day^{-1} (+15%), while P_{conv} decreases by −0.010 mm day^{-1} (−13%, discussed in Section 4.3).

The droplet number concentration N_c decreases due to dust-INP in agreement with the depletion in LWP. However, despite an increase in IWP the concentration of ice particles N_i decreases (discussed in Section 4.3).

In **NS-Tuned**, the magnitude of the cloud microphysical changes is dominated by the increase in dust-INP efficiency, while the large hemispheric asymmetry is due to the implementation of the dust threshold for droplet freezing. For the cloud water path, CC, CREs, and droplet concentration, the changes in both hemispheres are 2–3 times higher in **NS10K** compared to **NS** (see Table S2). For **NS-Tuned**, the changes due to dust-INP at 30°N–60°N are slightly lower (by −10% or less in magnitude) compared to **NS10K**. In contrast, at 30°S–60°S the changes for **NS-Tuned** are significantly lower (by −30% or more) compared to **NS10K** (see also supporting information S13).

4. Discussion

4.1. Dust-INP Versus Meteorological Impact on Cloud-Phase

Our simulations suggest that meteorology plays rather a minor role on cloud-phase variability. Meteorology could affect the formation and downward transport of ice clouds formed at temperatures colder than −35°C (without INP). However, the model results presented in Section 3.2 show that when immersion freezing is turned off, the hemispheric and seasonal contrasts in cloud top phase are very low (below 5%). These low contrasts suggest that the hemispheric and seasonal meteorology variability (including wind, humidity, and temperature) do not affect the cloud ice frequency. Furthermore, if dust-INP concentrations are held constant, the cloud-phase contrasts vanish as well (see supporting information S7), suggesting that cloud

glaciation at temperatures warmer than −35°C is controlled by dust-INP rather than by meteorology. In other words, at least in the model, the cloud-top-phase contrasts are controlled by the variability of dust-driven cloud glaciation at temperatures warmer than −35°C.

4.2. Liquid Water Depletion and Dust-Driven Glaciation in the LD Scheme

The stronger decrease in LWP in **LD** compared to **NS** is closely related to the variability of CCN. To explain the strong decrease in LWP due to dust-driven cloud glaciation in **LD**, we studied the effect of TKE and CCN on droplet freezing. In the LD scheme, both a higher TKE and a lower CCN lead to higher droplet freezing (see Equations 1 and 2). Sensitivity tests showed that the variability in TKE only plays a minor role on LWP. However, setting CCN to a constant—so that the CIF is similar to the default **LD** simulation—results in a weaker LWP reduction and weaker CRE increase due to dust-INP (see supporting information S6 and S10). This suggests that the CCN variability is responsible for the higher LWP depletion and higher CRE in **LD**, perhaps due to an unrealistic enhancement in droplet freezing during conditions of low CCN.

In addition, the lower hemispheric contrast in cloud-phase for **LD** compared to **NS** is unrelated to TKE and CCN and probably related to the prognostic formulation (time dependent) of the LD scheme. Other than for **NS**, the number of frozen droplets in **LD** can keep increasing with time as dust-INP are not depleted in the model after freezing (see Section 2.3).

4.3. Droplet Freezing and Precipitation

The high increase in P_{strat} at the expense of P_{conv} in **NS-Tuned** may be associated with the timing of droplet freezing events. If low INP concentrations are allowed to freeze droplets, the downward transport of ice particles may be too low for the hydrometeors to reach the surface without evaporating along the way, but will still deplete the water content of the cloud. In contrast, if low INP concentrations are not allowed to trigger freezing, more liquid content will be available for future droplet freezing events, which would lead more frequently to precipitation. This may also result in a lower water vapor content below the cloud at low dust conditions. Thus, during convection drier air would be entrained, which could explain the inhibition of P_{conv}. Alternatively, droplet freezing could change the temperature gradient, leading to a more stable atmosphere, suppressing convection.

The slight decrease in N_i due to dust-INP may be related to a lower number of droplets available for freezing at temperatures colder than −35°C, because they already freeze earlier at warmer temperatures. For temperatures warmer than −35°C, ice particles will grow by depleting existing cloud droplets. Therefore, despite an increase in IWP, heterogeneous freezing may cause N_i to decrease as fewer cloud droplets reach temperatures colder than −35°C.

4.4. A Misrepresented Ice Process?

As found with ECHAM-HAM and confirmed with the E3SM model (see Figure S2), a higher INP efficiency (**NS10K** compared to **NS**) leads to a better agreement between the cloud-phase contrasts and observations. Along the pathway between dust emission and cloud glaciation, several reasons could explain this behavior:

(a) **INP load.** ECHAM-HAM has shown a good agreement with both ground-based and spaceborne observations of dust loading (Koffi et al., 2016; Tegen et al., 2019). Nevertheless, biases in dust loading or size distribution may affect droplet freezing (Shi & Liu, 2019). In addition, coarse dust loading in models is thought to be underestimated, such that only 25% of the observed loading is represented (Adebiyi & Kok, 2020; Shi & Liu, 2019). Nevertheless, this bias is too low to alone explain the differences found in our results.

(b) **INP-to-Ice.** Efficient dust-INP containing about 20% K-feldspar can freeze at temperatures about +5 °C warmer compared to common dust-INP like montmorillonite (compare **NS** and A13 in Figure 1). Therefore, including additional dust mineral types (e.g., K-feldspar) in the simulation of INP concentrations could lead to a moderate improvement in the model (see **NS5K** in Figure S5). Alternatively, secondary ice production (Field et al., 2017; Lauber et al., 2018) could result in more ice particles per INP than expected. There are additional processes, such as INP preactivation (Wagner et al., 2016) or INP-recycling

(Solomon et al., 2015), which could also lead to an increased number of frozen droplets. In addition, dust aerosol could include other substances such as biogenic material, which could enhance its ice-nucleating efficiency (Augustin-Bauditz et al., 2016; Kanji et al., 2017; O'Sullivan et al., 2014, 2016).

(c) **Ice-to-Cloud Glaciation.** There could be a misrepresentation in the processes linking the ice number concentration with the glaciation of a mixed-phase cloud. For example, if the WBF process is underestimated, a higher droplet freezing will be needed in the model for clouds to glaciate. Additionally, collision and transport processes, such as ice–ice aggregation, riming, ice fragmenting, and ice sedimentation, also affect the number and size of ice particles in the cloud and how fast the cloud will glaciate (Korolev et al., 2017). These processes are parameterized differently in ECHAM-HAM and E3SM but lead to similar cloud-phase contrasts, suggesting that the differences in the ice microphysics schemes of these models affect the dust-driven glaciation to a minor degree. Nevertheless, other ice microphysics schemes may include more complex representations of the WBF process and secondary ice formation, which should be considered in future studies.

(d) **INP tracking.** In addition to a higher INP efficiency, setting a dust concentration threshold for droplet freezing in **NS-Tuned** inhibited much of the cloud glaciation in clean conditions such as in the southern midlatitudes, leading to more realistic cloud-phase contrasts. This suggests that—at least during low dust concentrations—INP concentrations may be overestimated due to the lack of INP depletion in climate models.

5. Conclusions

We showed that dust-driven droplet freezing can be evaluated in climate models using satellite observations of regional and seasonal contrasts in cloud ice frequency. We consider this an improvement from previous tuning strategies where only mean atmospheric state quantities like cloud ice frequency or dust-INP concentrations are constrained.

Observations of cloud-phase contrast may provide a reference for the effect of dust-INP on radiation and precipitation. With the NS-Tuned simulation, which is constrained by observations, the simulated radiative effect of cloud glaciation is much lower ($+0.14 \pm 0.13$ W m^{-2}) than for the default LD scheme ($+1.48 \pm 0.16$ W m^{-2}) at 30°N–60°N. We attribute this difference to an overestimation of water depletion due to dust-INP in the default scheme. Our study suggests that dust-driven cloud glaciation can be trusted only in models, which are able to reproduce both the observed mean-state cloud-phase partitioning and cloud-phase contrasts. These new constraints on the impact of dust-INP on climate may help to better understand climate change under varying aerosol loadings and direct modeling efforts in the right direction.

Conflict of Interest

The authors declare no conflicts of interest relevant to this study.

Data Availability Statement

The data set containing the GDP ensemble and CALIPSO-GOCCP regridded product can be found at https://catalogue.ceda.ac.uk/uuid/f742c505c935467ebb4cf89a611a4436. The results of the ECHAM-HAM simulations can be found at https://zenodo.org/record/4836345#.YLDxti0RrRb.

Acknowledgments
We thank the HAMMOZ community for providing access to the ECHAM-HAM model and the DKRZ for providing computational resources. We thank Jan Kretzschmar and the Max Planck Institute for providing an implementation of COSP 2.1 for the ECHAM-HAM. We also thank Prof. Ulrike Lohmann for helpful discussion. See additional acknowledgments in Text S1. Open access funding enabled and organized by Projekt DEAL.

References

Adebiyi, A. A., & Kok, J. F. (2020). Climate models miss most of the coarse dust in the atmosphere. *Science Advances*, *6*(15), eaaz9507. https://doi.org/10.1126/sciadv.aaz9507

Albrecht, B. A. (1989). Aerosols, cloud microphysics, and fractional cloudiness. *Science*, *245*(4923), 1227–1230. https://doi.org/10.1126/science.245.4923.1227

Atkinson, J. D., Murray, B. J., Woodhouse, M. T., Whale, T. F., Baustian, K. J., Carslaw, K. S., et al. (2013). The importance of feldspar for ice nucleation by mineral dust in mixed-phase clouds. *Nature*, *498*(7454), 355–358. https://doi.org/10.1038/nature12278

Augustin-Bauditz, S., Wex, H., Denjean, C., Hartmann, S., Schneider, J., Schmidt, S., et al. (2016). Laboratory-generated mixtures of mineral dust particles with biological substances: Characterization of the particle mixing state and immersion freezing behavior. *Atmospheric Chemistry and Physics*, *16*(9), 5531–5543. https://doi.org/10.5194/acp-16-5531-2016

Bellouin, N., Quaas, J., Gryspeerdt, E., Kinne, S., Stier, P., Watson-Parris, D., et al. (2020). Bounding global aerosol radiative forcing of climate change. *Reviews of Geophysics*, *58*, e2019RG000660. https://doi.org/10.1029/2019RG000660

Bergeron, T. (1935). On the physics of cloud and precipitation. *Proceedings of the Fifth Assembly of the International Union of Geodesy and Geophysics*, *2*, 156–178.

Bruno, O., Hoose, C., Storelvmo, T., Coopman, Q., & Stengel, M. (2021). Exploring the cloud top phase partitioning in different cloud types using active and passive satellite sensors. *Geophysical Research Letters*, *48*, e2020GL089863. https://doi.org/10.1029/2020GL089863

Cesana, G., & Chepfer, H. (2013). Evaluation of the cloud thermodynamic phase in a climate model using CALIPSO-GOCCP. *Journal of Geophysical Research: Atmospheres*, *118*, 7922–7937. https://doi.org/10.1002/jgrd.50376

Chepfer, H., Bony, S., Winker, D., Cesana, G., Dufresne, J. L., Minnis, P., et al. (2010). The GCM-oriented CALIPSO cloud product (CALIPSO-GOCCP). *Journal of Geophysical Research*, *115*, D00H16. https://doi.org/10.1029/2009JD012251

Claquin, T., Schulz, M., & Balkanski, Y. J. (1999). Modeling the mineralogy of atmospheric dust sources. *Journal of Geophysical Research*, *104*(D18), 22243–22256. https://doi.org/10.1029/1999JD900416

Connolly, P. J., Möhler, O., Field, P. R., Saathoff, H., Burgess, R., Choularton, T., & Gallagher, M. (2009). Studies of heterogeneous freezing by three different desert dust samples. *Atmospheric Chemistry and Physics*, *9*(8), 2805–2824. https://doi.org/10.5194/acp-9-2805-2009

Cowie, S. M., Knippertz, P., & Marsham, J. H. (2014). A climatology of dust emission events from Northern Africa using long-term surface observations. *Atmospheric Chemistry and Physics*, *14*(16), 8579–8597. https://doi.org/10.5194/acp-14-8579-2014

Cziczo, D. J., Froyd, K. D., Gallavardin, S. J., Moehler, O., Benz, S., Saathoff, H., & Murphy, D. M. (2009). Deactivation of ice nuclei due to atmospherically relevant surface coatings. *Environmental Research Letters*, *4*(4), 044013. https://doi.org/10.1088/1748-9326/4/4/044013

DeMott, P. J., Prenni, A. J., Liu, X., Kreidenweis, S. M., Petters, M. D., Twohy, C. H., et al. (2010). Predicting global atmospheric ice nuclei distributions and their impacts on climate. *Proceedings of the National Academy of Sciences of the United States of America*, *107*(25), 11217–11222. https://doi.org/10.1073/pnas.0910818107

Dietlicher, R., Neubauer, D., & Lohmann, U. (2018). Prognostic parameterization of cloud ice with a single category in the aerosol–climate model ECHAM(v6.3.0)-HAM(v2.3). *Geoscientific Model Development*, *11*(4), 1557–1576. https://doi.org/10.5194/gmd-11-1557-2018

Dietlicher, R., Neubauer, D., & Lohmann, U. (2019). Elucidating ice formation pathways in the aerosol–climate model ECHAM6-HAM2. *Atmospheric Chemistry and Physics*, *19*(14), 9061–9080. https://doi.org/10.5194/acp-19-9061-2019

Field, P. R., Lawson, R. P., Brown, P. R. A., Lloyd, G., Westbrook, C., Moisseev, D., et al. (2017). Secondary ice production: Current state of the science and recommendations for the future. *Meteorological Monographs*, *58*, 7.1–7.20. https://doi.org/10.1175/AMSMONOGRAPHS-D-16-0014.1

Findeisen, W., Volken, E., Giesche, A. M., & Brönnimann, S. (2015). Colloidal meteorological processes in the formation of precipitation. *Meteorologische Zeitschrift*, *24*(4), 443–454. https://doi.org/10.1127/metz/2015/0675

Forbes, R. M., & Ahlgrimm, M. (2014). On the representation of high-latitude boundary layer mixed-phase cloud in the ECMWF global model. *Monthly Weather Review*, *142*(9), 3425–3445. https://doi.org/10.1175/MWR-D-13-00325.1

Harrison, A. D., Lever, K., Sanchez-Marroquin, A., Holden, M. A., Whale, T. F., Tarn, M. D., et al. (2019). The ice-nucleating ability of quartz immersed in water and its atmospheric importance compared to K-feldspar. *Atmospheric Chemistry and Physics*, *19*(17), 11343–11361. https://doi.org/10.5194/acp-19-11343-2019

Hoose, C., Kristjánsson, J. E., Chen, J.-P., & Hazra, A. (2010). A classical-theory-based parameterization of heterogeneous ice nucleation by mineral dust, soot, and biological particles in a global climate model. *Journal of the Atmospheric Sciences*, *67*(8), 2483–2503. https://doi.org/10.1175/2010JAS3425.1

Hoose, C., Lohmann, U., Erdin, R., & Tegen, I. (2008). The global influence of dust mineralogical composition on heterogeneous ice nucleation in mixed-phase clouds. *Environmental Research Letters*, *3*(2), 025003. https://doi.org/10.1088/1748-9326/3/2/025003

Hoose, C., & Möhler, O. (2012). Heterogeneous ice nucleation on atmospheric aerosols: A review of results from laboratory experiments, *Atmospheric Chemistry and Physics*, *12*(20), 9817–9854. https://doi.org/10.5194/acp-12-9817-2012

Hu, Y., Rodier, S., Xu, K. M., Sun, W., Huang, J., Lin, B., et al. (2010). Occurrence, liquid water content, and fraction of supercooled water clouds from combined CALIOP/IIR/MODIS measurements. *Journal of Geophysical Research*, *115*, D00H34. https://doi.org/10.1029/2009JD012384

Huang, W., Ickes, L., Tegen, I., Rinaldi, M., Ceburnis, D., & Lohmann, U. (2018). Global relevance of marine organic aerosol as ice nucleating particles. *Atmospheric Chemistry and Physics*, *18*(15), 11423–11445. https://doi.org/10.5194/acp-18-11423-2018

Ickes, L. (2015). *Using classical nucleation theory for parameterizing immersion freezing in mixed-phase clouds in global climate models* (Doctoral dissertation). Zürich, Switzerland: ETH Zurich. https://doi.org/10.3929/ethz-a-010564637

Ickes, L., Welti, A., & Lohmann, U. (2017). Classical nucleation theory of immersion freezing: Sensitivity of contact angle schemes to thermodynamic and kinetic parameters. *Atmospheric Chemistry and Physics*, *17*(3), 1713–1739. https://doi.org/10.5194/acp-17-1713-2017

IPCC; Chidthaisong, A., Ciais, P., Cox, P., Dickinson, R., Hauglustaine, D., & Zhang, X. (2007). *Climate change 2007: Working Group I: The physical science basis* (Tech. Rep.).

Kanji, Z. A., Ladino, L. A., Wex, H., Boose, Y., Burkert-Kohn, M., Cziczo, D. J., & Krämer, M. (2017). Overview of ice nucleating particles. *Meteorological Monographs*, *58*, 1.1–1.3. https://doi.org/10.1175/amsmonographs-d-16-0006.1

Kawamoto, K., Yamauchi, A., Suzuki, K., Okamoto, H., & Li, J. (2020). Effect of dust load on the cloud top ice–water partitioning over northern middle to high latitudes with CALIPSO products. *Geophysical Research Letters*, *47*, e2020GL088030. https://doi.org/10.1029/2020GL088030

Koffi, B., Schulz, M., Bréon, F.-M., Dentener, F., Steensen, B. M., Griesfeller, J., et al. (2016). Evaluation of the aerosol vertical distribution in global aerosol models through comparison against CALIOP measurements: AeroCom phase II results. *Journal of Geophysical Research: Atmospheres*, *121*, 7254–7283. https://doi.org/10.1002/2015JD024639

Korolev, A., McFarquhar, G., Field, P. R., Franklin, C., Lawson, P., Wang, Z., et al. 2017). Mixed-phase clouds: Progress and challenges. *Meteorological Monographs*, *58*, 5.1–5.50. https://doi.org/10.1175/amsmonographs-d-17-0001.1

Lauber, A., Kiselev, A., Pander, T., Handmann, P., & Leisner, T. (2018). Secondary ice formation during freezing of levitated droplets. *Journal of the Atmospheric Sciences*, *75*(8), 2815–2826. https://doi.org/10.1175/JAS-D-18-0052.1

Lohmann, U., & Diehl, K. (2006). Sensitivity studies of the importance of dust ice nuclei for the indirect aerosol effect on stratiform mixed-phase clouds. *Journal of the Atmospheric Sciences*, *63*(3), 968–982. https://doi.org/10.1175/JAS3662.1

Lohmann, U., Stier, P., Hoose, C., Ferrachat, S., Kloster, S., Roeckner, E., & Zhang, J. (2007). Cloud microphysics and aerosol indirect effects in the global climate model ECHAM5-HAM. *Atmospheric Chemistry and Physics*, *7*(13), 3425–3446. https://doi.org/10.5194/acp-7-3425-2007

McCoy, D. T., Tan, I., Hartmann, D. L., Zelinka, M. D., & Storelvmo, T. (2016). On the relationships among cloud cover, mixed-phase partitioning, and planetary albedo in GCMs. *Journal of Advances in Modeling Earth Systems*, *8*, 650–668. https://doi.org/10.1002/2015MS000589

Morrison, H., & Milbrandt, J. A. (2015). Parameterization of cloud microphysics based on the prediction of bulk ice particle properties. Part I: Scheme description and idealized tests. *Journal of the Atmospheric Sciences*, *72*(1), 287–311. https://doi.org/10.1175/JAS-D-14-0065.1

Mülmenstädt, J., Nam, C., Salzmann, M., Kretzschmar, J., L'Ecuyer, T. S., Lohmann, U., et al. (2020). Reducing the aerosol forcing uncertainty using observational constraints on warm rain processes. *Science Advances*, *6*(22), eaaz6433. https://doi.org/10.1126/sciadv.aaz6433

Murray, B. J., Carslaw, K. S., & Field, P. R. (2021). Opinion: Cloud-phase climate feedback and the importance of ice-nucleating particles. *Atmospheric Chemistry and Physics*, *21*(2), 665–679. https://doi.org/10.5194/acp-21-665-2021

Neubauer, D., Ferrachat, S., Siegenthaler-Le Drian, C., Stier, P., Partridge, D. G., Tegen, I., et al. (2019). The global aerosol–climate model ECHAM6.3-HAM2.3—Part 2: Cloud evaluation, aerosol radiative forcing, and climate sensitivity. *Geoscientific Model Development*, *12*(8), 3609–3639. https://doi.org/10.5194/gmd-12-3609-2019

Niemand, M., Möhler, O., Vogel, B., Vogel, H., Hoose, C., Connolly, P., et al. (2012). A particle-surface-area-based parameterization of immersion freezing on desert dust particles. *Journal of the Atmospheric Sciences*, *69*(10), 3077–3092. https://doi.org/10.1175/JAS-D-11-0249.1

O'Sullivan, D., Murray, B. J., Malkin, T. L., Whale, T. F., Umo, N. S., Atkinson, J. D., et al. (2014). Ice nucleation by fertile soil dusts: Relative importance of mineral and biogenic components. *Atmospheric Chemistry and Physics*, *14*(4), 1853–1867. https://doi.org/10.5194/acp-14-1853-2014

O'Sullivan, D., Murray, B. J., Ross, J. F., & Webb, M. E. (2016). The adsorption of fungal ice-nucleating proteins on mineral dusts: A terrestrial reservoir of atmospheric ice-nucleating particles. *Atmospheric Chemistry and Physics*, *16*(12), 7879–7887. https://doi.org/10.5194/acp-16-7879-2016

Rasch, P. J., Xie, S., Ma, P.-l., Lin, W., Wang, H., Tang, Q., et al. (2019). An overview of the atmospheric component of the Energy Exascale Earth System Model. *Journal of Advances in Modeling Earth Systems*, *11*, 2377–2411. https://doi.org/10.1029/2019MS001629

Seinfeld, J. H., Bretherton, C., Carslaw, K. S., Coe, H., DeMott, P. J., Dunlea, E. J., et al. (2016). Improving our fundamental understanding of the role of aerosol–cloud interactions in the climate system. *Proceedings of the National Academy of Sciences of the United States of America*, *113*(21), 5781–5790. https://doi.org/10.1073/pnas.1514043113

Shi, Y., & Liu, X. (2019). Dust radiative effects on climate by glaciating mixed-phase clouds. *Geophysical Research Letters*, *46*, 6128–6137. https://doi.org/10.1029/2019GL082504

Solomon, A., Feingold, G., & Shupe, M. D. (2015). The role of ice nuclei recycling in the maintenance of cloud ice in arctic mixed-phase stratocumulus. *Atmospheric Chemistry and Physics*, *15*(18), 10631–10643. https://doi.org/10.5194/acp-15-10631-2015

Stanelle, T., Bey, I., Raddatz, T., Reick, C., & Tegen, I. (2014). Anthropogenically induced changes in twentieth century mineral dust burden and the associated impact on radiative forcing. *Journal of Geophysical Research: Atmospheres*, *119*, 13526–13546. https://doi.org/10.1002/2014JD022062

Swales, D. J., Pincus, R., & Bodas-Salcedo, A. (2018). The cloud feedback model intercomparison project observational simulator package: Version 2. *Geoscientific Model Development*, *11*(1), 77–81. https://doi.org/10.5194/gmd-11-77-2018

Tan, I., Storelvmo, T., & Choi, Y. S. (2014). Spaceborne lidar observations of the ice-nucleating potential of dust, polluted dust, and smoke aerosols in mixed-phase clouds. *Journal of Geophysical Research: Atmospheres*, *119*, 6653–6665. https://doi.org/10.1002/2013JD021333

Tan, I., Storelvmo, T., & Zelinka, M. D. (2016). Observational constraints on mixed-phase clouds imply higher climate sensitivity. *Science*, *352*(6282), 224–227. https://doi.org/10.1126/science.aad5300

Tegen, I., Neubauer, D., Ferrachat, S., Drian, C. S. L., Bey, I., Schutgens, N., et al. (2019). The global aerosol–climate model ECHAM6.3-HAM2.3—Part 1: Aerosol evaluation. *Geoscientific Model Development*, *12*(4), 1643–1677. https://doi.org/10.5194/gmd-12-1643-2019

Twomey, S. (1974). Pollution and the planetary albedo. *Atmospheric Environment*, *8*(12), 1251–1256. https://doi.org/10.1016/0004-6981(74)90004-3

Ullrich, R., Hoose, C., Möhler, O., Niemand, M., Wagner, R., Höhler, K., et al. (2017). A new ice nucleation active site parameterization for desert dust and soot. *Journal of the Atmospheric Sciences*, *74*(3), 699–717. https://doi.org/10.1175/jas-d-16-0074.1

Vergara-Temprado, J., Murray, B. J., Wilson, T. W., O'Sullivan, D., Browse, J., Pringle, K. J., et al. (2017). Contribution of feldspar and marine organic aerosols to global ice nucleating particle concentrations. *Atmospheric Chemistry and Physics*, *17*(5), 3637–3658. https://doi.org/10.5194/acp-17-3637-2017

Villanueva, D., Heinold, B., Seifert, P., Deneke, H., Radenz, M., & Tegen, I. (2020). The day-to-day co-variability between mineral dust and cloud glaciation: A proxy for heterogeneous freezing. *Atmospheric Chemistry and Physics*, *20*(4), 2177–2199. https://doi.org/10.5194/acp-20-2177-2020

Villanueva, D., Senf, F., & Tegen, I. (2021). Hemispheric and seasonal contrast in cloud thermodynamic phase from A-Train spaceborne instruments. *Journal of Geophysical Research: Atmospheres*, *126*, e2020JD034322. https://doi.org/10.1029/2020JD034322

Wagner, R., Kiselev, A., Moehler, O., Saathoff, H., & Steinke, I. (2016). Pre-activation of ice-nucleating particles by the pore condensation and freezing mechanism. *Atmospheric Chemistry and Physics*, *16*(4), 2025–2042. https://doi.org/10.5194/acp-16-2025-2016

Wegener, A. (1911). *Thermodynamik der Atmosphäre*. Leipzig, Germany: J.A. Barth.

Wu, M., Liu, X., Yu, H., Wang, H., Shi, Y., Yang, K., et al. (2020). Understanding processes that control dust spatial distributions with global climate models and satellite observations. *Atmospheric Chemistry and Physics*, *20*(22), 13835–13855. https://doi.org/10.5194/acp-20-13835-2020

Yun, Y., & Penner, J. E. (2013). An evaluation of the potential radiative forcing and climatic impact of marine organic aerosols as heterogeneous ice nuclei. *Geophysical Research Letters*, *40*, 4121–4126. https://doi.org/10.1002/grl.50794

Yun, Y., Penner, J. E., & Popovicheva, O. (2013). The effects of hygroscopicity on ice nucleation of fossil fuel combustion aerosols in mixed-phase clouds. *Atmospheric Chemistry and Physics*, *13*(8), 4339–4348. https://doi.org/10.5194/acp-13-4339-2013

Zhang, D., Wang, Z., Kollias, P., Vogelmann, A. M., Yang, K., & Luo, T. (2018). Ice particle production in mid-level stratiform mixed-phase clouds observed with collocated A-Train measurements. *Atmospheric Chemistry and Physics*, *18*(6), 4317–4327. https://doi.org/10.5194/acp-18-4317-2018